AAPS PharmSciTech, Vol. 19, No. 7, October 2018 (© 2018)
DOI: 10.1208/s12249-018-1121-1

Research Article

Theme: Team Science and Education for Pharmaceuticals: the NIPTE Model
Guest Editors: Ajaz S. Hussain, Kenneth Morris, and Vadim J. Gurvich

Particle Size Distribution Equivalency as Novel Predictors for Bioequivalence

Pratak Ngeacharernkul,[1] Stephen D. Stamatis,[1,2] and Lee E. Kirsch[1,3]

Received 17 May 2018; accepted 6 July 2018; published online 16 August 2018

Abstract. The use of particle size distribution (PSD) similarity metrics and the development and incorporation of drug release predictions based on PSD properties into PBPK models for various drug administration routes may provide a holistic approach for evaluating the effect of PSD differences on *in vitro* drug release and bioavailability of disperse systems. The objectives of this study were to provide a rational approach for evaluating the utility of *in vitro* PSD comparators for predicting bioequivalence for subcutaneously administered test and reference drug emulsions. Two types of *in vitro* comparators for test and reference emulsion products were evaluated: PSD characterization comparators (overlap metrics, median, and span ratios) and release profile comparators (f_2 and various fractional time ratios). A subcutaneous-input PBPK disposition model was developed to simulate blood concentration-time profiles of reference and test emulsion products and pharmacokinetic responses (*e.g.*, AUC, C_{max}, and T_{max}) were used to determine bioequivalence. A pool of 10,440 pairs of test and reference products was simulated using Monte Carlo experiments. The PSD and release profile comparators were correlated to pass/fail bioequivalence metrics using logistical regression. Based on the use of single *in vitro* comparators, the f_2 method was the best predictor of bioequivalence prediction. The use of combinations of f_2 and PSD overlap comparators (*e.g.*, OVL or PROB) improved bioequivalence prediction to about 90%. Simulation procedures used in this study demonstrated a process for developing reliable *in vitro* BE predictors.

KEY WORDS: bioequivalence; particle size distribution; modeling and simulation; emulsion; subcutaneous administration; PBPK.

INTRODUCTION

Particle size (PS) and particle size distribution (PSD) are critical quality attributes for numerous pharmaceutical dosage forms including solid oral products; dispersed systems (injectable, oral, and topical) as well as particulate-based inhaled products (1). The key efficacy and safety performance attributes associated with PS and PSD include the deposition of inhaled particulates; the release rate of immediate-, extended-, and controlled-release products; drug targeting of stealth parenterals; and the safety of intravenous emulsion products wherein a sub-population of large particles may create some risk of pulmonary embolism. In addition, PSD properties can play an important role in the manufacturing of pharmaceutical products (*e.g.*, powder flow and blending) and in drug stability both physical, such as coalescence and/or caking of dispersed systems, and chemical instability of particulate-based solids.

In the licensure of a generic drug product *via* the abbreviated new drug application (ANDA) process, both pharmaceutical equivalence and bioequivalence (BE) of the generic drug product must be established for the US-FDA licensure approval. A single-dose pharmacokinetic study using a non-replicate crossover study design is used to evaluate BE. Pharmacokinetic (PK) parameters (*e.g.*, C_{max}, T_{max}, $AUC_{0\text{-}t}$, and $AUC_{0\text{-}\infty}$) are determined for test and reference drug products and BE is demonstrated if the 90% confidence intervals of test and reference PK parameters are within 80 and 125% (2). The FDA has also suggested an approach for comparing drug products based on their particle size distribution similarity for bioequivalence waiver using a comparison of median (D_{50}) and span $\left(\frac{D_{90}-D_{10}}{D_{50}}\right)$ values between products or batches (3).

Our research objectives were to evaluate the utility of various PSD-based metrics for predicting pharmacokinetic-

Guest Editors: Ajaz S. Hussain, Kenneth Morris, and Vadim J. Gurvich

[1] Division of Pharmaceutics, The University of Iowa, Iowa City, Iowa, USA.
[2] *Present Address:* Lilly Research Laboratories, Eli Lilly and Company, Indianapolis, Indiana, USA.
[3] To whom correspondence should be addressed. (e–mail: lee-kirsch@uiowa.edu)

based BE by developing simulation models for subcutaneous drug release from emulsions coupled with PBPK pharmacokinetic disposition models to specifically account for the effects of PSD on BE. The central questions are whether bioequivalence can be predicted based on PSD comparisons and what *in vitro* metric or combination of metrics can provide the most reliable BE predictions?

The general approach (Fig. 1) was to create reference and test emulsion product pairs wherein the drug substance properties were randomly selected from representative compilations of published drug substance properties. The drug substance properties including diffusion coefficient, partition coefficient, and subcutaneous-input parameters were the same for both reference and test drug products within the same pair. However, the particle size distribution properties of reference and test drug products within each pair randomly differed.

Over 10,000 pairs of reference and test drug products were constructed. For each pair, PSD metrics (*e.g.*, median size, span, and overlap metrics) and *in vitro* release rate metrics (*e.g.*, similarity factor [f_2], fractional time ratios) were estimated. In addition, bioequivalence metrics were computed from simulated blood concentration-time profiles for each product pair. The utility of the PSD-based metrics (both PSD and *in vitro* release rate comparators) for predicting pharmacokinetic-based BE was evaluated by determining the correlation between them using logistical regression.

METHODS

Modeling Methodology

Three models were used: PSD model, drug release model, and subcutaneous-input PBPK model. Particle size distributions for reference (RLS) and test (generic) drug products were generated using the PSD model which were then used in the drug release model to generate release profiles which in turn were used for drug input in the PBPK models to provide drug exposure profiles.

PSD Model

A skew-normal distribution was employed to generate PSDs (4); the density function for a random variable Z with a shape parameter α at any given z and α can be expressed as:

$$f(z) = 2\,\frac{1}{\sqrt{2\pi}} e^{\left(-z^2/2\right)} \int_{-\infty}^{\alpha z} \frac{1}{\sqrt{2\pi}}\, e^{\left(-t^2/2\right)} dt. \tag{1}$$

In general, the skew-normal distribution is a probability distribution extended from a normal distribution by adding an additional shape parameter in order to reflect the "skewness" of the distribution. A normal distribution is a special case of the skew-normal distribution wherein the shape parameter is 0. Therefore, the skew-normal distribution has a number of properties which are similar to the standard normal distribution; for example, both distributions are unimodal, they support continuous random variable, and a square of a skew-normal variable is a chi-square variable with one degree of freedom (4). For any skew-normal random variable Z with skew parameter α, the cumulative distribution of Z is given by

$$P(Z \le y) = \int_{-\infty}^{y} \frac{1}{\pi}\, e^{\left(-z^2/2\right)} \int_{-\infty}^{\alpha z} e^{\left(-t^2/2\right)} dt\, dz. \tag{2}$$

Although the random variable Z and $f(z)$ are the basic components to construct a skew-normal distribution, location (ξ) and scale (σ) parameters are used to define distribution characteristics. The variable Z can be transformed using those two parameters and a linear transformation to obtain a random variable X which has a skew-normal distribution with three parameters: location, scale, and shape and can be written as $X \sim \mathrm{SN}(\xi, \sigma^2, \alpha)$

$$X = \xi + \sigma Z. \tag{3}$$

After a substitution of random variable Z with random variable X in the Eq. 1, the probability density function of random variable X with location, scale, and shape parameters becomes

$$\begin{aligned} f(x) &= \frac{2}{\sigma}\phi\left(\frac{x-\xi}{\sigma}\right)\Phi\left(\alpha\left(\frac{x-\xi}{\sigma}\right)\right) \\ &= \frac{1}{\sigma\sqrt{2\pi}} e^{-\frac{1}{2}\left(\frac{x-\xi}{\sigma}\right)^2} erfc\left(-\frac{\alpha}{\sqrt{2}}\left(\frac{x-\xi}{\sigma}\right)\right). \end{aligned} \tag{4}$$

The skew-normal distributions for test and reference products were constructed by selecting different values for these three parameters for each product.

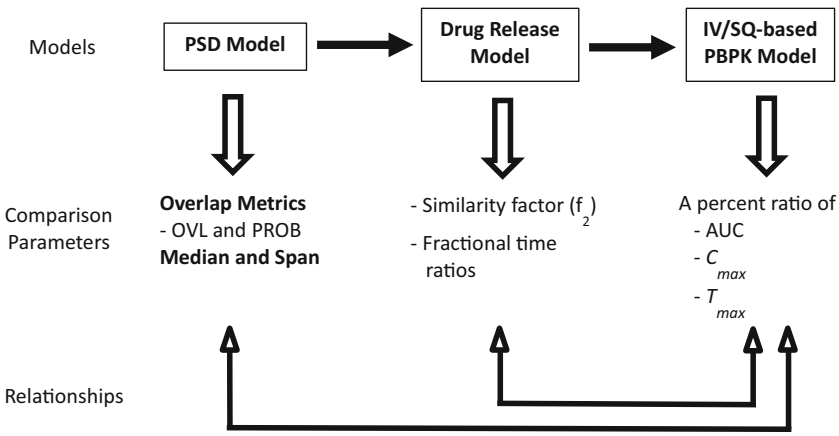

Fig. 1. Overview of methods for evaluating the relationship between *in vitro* comparators and pharmacokinetic bioequivalence metrics

Drug Release Model

The model of Bikhazi and Higuchi (5) was used to describe the rate of drug concentration decrease within a single droplet of radius r_i based on the following equation:

$$\frac{dC_i}{dt} = \frac{3 \cdot D \cdot P\left(C_{bulk} - \frac{C_i}{K}\right)}{r_i(D + r_i \cdot P)} \tag{5}$$

where C_i is the concentration of drug within a single droplet of radius r_i; t is time; C_{bulk} is the concentration in the bulk dissolution medium; D is the diffusion coefficient; P is the permeability coefficient; K is the oil:water partition coefficient.

Emulsion formulations are polydisperse systems where particles of various sizes are dispersed in a medium. Equation 5 only describes the release rate from a monodisperse system, and therefore it was modified to account for the overall release rate from polydisperse systems. The key assumptions were sink conditions, diffusion-controlled release, and a common initial drug concentration in all droplets. Application of these assumptions resulted in the following equation which describes the time-dependent drug concentration in each droplet.

$$\frac{dC_i}{dt} = -\frac{3 \cdot D \cdot C_i}{K \cdot r_i^2}. \tag{6}$$

The time-dependent concentration can be described by exponential decay where C_0 is the initial droplet drug concentration.

$$C_i(t) = C_0 e^{-\frac{3 \cdot D}{K \cdot r_i^2} t}. \tag{7}$$

The overall release was computed by summing across the PSD and the total mass of drug that remains in the droplets at time t is given by

$$M(t) = \sum_{i=1}^{n} N_i V_i C_i(t) \tag{8}$$

where M(t) is the total mass of drug that remains in the droplets at time t; N_i is the number of droplet in size range i; V_i is the volume of droplet in size range i. As a result, the total amount of drug at time 0 is given by

$$M_{\text{tot}} = \sum_{i=1}^{n} N_i V_i C_0. \tag{9}$$

The cumulative percentage released as a function of time is given by

$$R(t) = 100\left(1 - \frac{\sum_{i=1}^{n} N_i V_i C_i(t)}{M_{\text{tot}}}\right). \tag{10}$$

By substituting Eqs. 7 and 9 into Eq. 10, the volume of particles at particular size by $\frac{4}{3}\pi r_i^3$ assuming all particles are spherical the following equation can be obtained:

$$R(t) = 100\left(1 - \frac{\sum_{i=1}^{n} N_i r_i^3 e^{-\frac{3 \cdot D}{K \cdot r_i^2} t}}{\sum_{j=1}^{n} N_j r_j^3}\right) \tag{11}$$

which can be simplified by noting,

$$\frac{N_i r_i^3}{\sum_{j=1}^{n} N_j r_j^3} = \text{volume fraction of } r_i \ (f_{Vi}) \tag{12}$$

so that,

$$R(t) = 100\left(1 - \sum_{i=1}^{n} f_{Vi} e^{-\frac{3 \cdot D}{K \cdot r_i^2} t}\right). \tag{13}$$

R codes were written based on the equations above for simulating release profiles of reference and test drug products with different PSDs (R Core Team [2017] URL https://www.R-project.org/).

PBPK Model

Three sub-models were combined to provide blood concentration-time profiles for pairs of reference and test drug products: emulsion drug release profiles, subcutaneous-input model, and PKPB disposition model.

The simulation of drug release for a polydisperse emulsion using the Bikhazi and Higuchi model (Eq. 6) was conducted by dividing the PSD into 32 particle size bins. Particles in each bin were assumed to have the same size and each particle size bin was independent. As a result, the amount of drug released from particles in each bin was calculated using the following equations:

$$V_i = \frac{4}{3}\,\pi\, r_i^3 \tag{14}$$

$$N_i = \left(\frac{\text{TotalDose}}{\text{Density}} \cdot V_{\text{frac}(i)}\right) / V_i \tag{15}$$

$$\frac{dX_i}{dt} = V_i \cdot N_i \cdot \left(\frac{3 \cdot D \cdot C_i}{K \cdot r^2}\right) \tag{16}$$

where V_i is the volume of droplets with radius i in liter (L); N_i is the number of droplets with radius i; TotalDose is a total mass of internal phase injected in milligram; Density is an internal phase density in milligram/liter; $V_{\text{frac}(i)}$ is a volume fraction of droplet with radius i; X_i is an amount of drug released from droplet with radius i. To find the total drug release at each time point, amount of drug released from droplets size i at each time point was summed.

In the subcutaneous model (Fig. 2), an input compartment was defined as a volume of the SQ tissue ten times larger than an injection volume of drug in accordance with

the literature (6). Since a maximum subcutaneous injection volume is about 2 mL (7), the dose was fixed at 1 mL of 140 mg drug. Drug released from emulsion droplets was assumed to be absorbed into a vein by a first order rate process (subcutaneous permeability constant; k_{SQ}). In addition, released drug was assumed to undergo first pass loss at the injection site at a rate which was a fraction of subcutaneous permeability constant ($k_{SQ\_Eli} = EF \times k_{SQ}$ when EF is an elimination fraction).

The rate of change of drug concentrations in the subcutaneous compartment is given by the following:

$$\frac{dC_{SQ}}{dt} = \frac{\text{TotalReleaseRate}}{V_{SQ}} - k_{SQ} \cdot C_{SQ} - EF \cdot k_{SQ} \cdot C_{SQ} \quad (17)$$

A PBPK disposition model (8) was used to predict drug concentration-time profiles after SQ administration. The model consists of 14 compartments which represent major organs/tissues such as lungs, adipose tissues, muscle, heart, brain, spleen, pancreas, liver, gut, stomach, bone, skin, thymus, and kidney. Each compartment was connected to arterial and venous blood compartments.

The rate and extent of drug concentration change in each compartment was described by a series of 17 differential equations (8). Reported organ tissue volumes and blood flows of each organ were based on 70 kg adult healthy males with the age in a range of 20–50 years (8,9). Drug compound-specific parameters required to populate the PBPK model were based on the IV-emulsion drug, propofol. These parameters include molecular weight (178 Da), solubility (124 mg/L), pKa (11), diffusion coefficient (7.07×10^{-6} cm^2/s), log $P_{o/w}$ (3.83), density (0.9533 g/mL), blood:plasma ratio (0.88), and plasma protein binding (0.985) (10–13). Intrinsic renal and hepatic clearance values were estimated from published hepatocyte and human kidney microsome depletion studies (14).

Tissue to plasma partition coefficients (K_{pu}) is the ratio of unbound drug concentration in tissues (C_T) to unbound drug concentration in plasma (C_{Up}) at steady state. According to Rodgers and Rowland (15,16), K_{pu} in each organ can be calculated using the following equation:

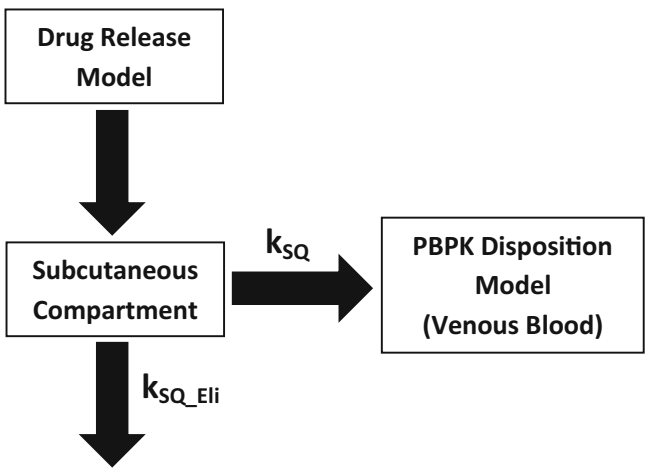

Fig. 2. Subcutaneous-input model

$$K_{pu} = \frac{C_T}{C_{Up}} = \frac{(C_{U,IW} \cdot f_{IW} + (C_{U,EW} + C_{PR,EW}) \cdot f_{EW} + C_{NL} \cdot f_{NL} + C_{NP} \cdot f_{NP})}{C_{Up}} \quad (18)$$

where f is fractional tissue volume; and IW, EW, NL, NP, and PR are intracellular water, extracellular water, neutral lipid, neutral phospholipid and protein, respectively.

The concentrations of unbound drug in the intracellular water ($C_{U,\,IW}$), the neutral lipid (C_{NL}) and neutral phospholipid (C_{NP}) can be calculated using the following three equations where P is the partition coefficient of the unionized drug; X and Y are different based on drug property as follows: for very weak monoprotic bases $X = 1 + 10^{pK_a - pH_{IW}}$ and $Y = 1 + 10^{pK_a - pH_p}$; for monoprotic acids $X = 1 + 10^{pH_{IW} - pK_a}$ and $Y = 1 + 10^{pH_p - pK_a}$; for neutral compounds X and $Y = 1$; and for zwitteric ions $X = 1 + 10^{pKa_{Base} - pH_{IW}} + 10^{pH_{IW} - pKa_{Acid}}$ and $Y = 1 + 10^{pKa_{Base} - pH_p} + 10^{pH_p - pKa_{Acid}}$ where pH_p and pH_{IW} are plasma and intracellular water pH, respectively.

$$C_{U,IW} = C_{Up} \cdot \frac{X}{Y} \quad (19)$$

$$C_{NL} = \frac{P \cdot C_{Up}}{Y} \quad (20)$$

$$C_{NP} = \frac{C_{Up}}{Y} \cdot (0.3P + 0.7) \quad (21)$$

The drug concentration in the extracellular water was calculated using the following equation:

$$C_{U,EW} + C_{PR,EW} = Cu_p + \left(\frac{Cu_p \cdot Ka_{PR} \cdot PR_T}{f_{EW}} \right) \quad (22)$$

assuming C_{Up} is equal to $C_{U,EW}$, albumin is a dominant binding protein, and Ka_{PR}, the association constant of acid and very weak bases for albumin and neutral drugs for lipoproteins, is identical in all tissues and equal to $\left[\frac{1}{f_u} - 1 - \left(\frac{P \cdot f_{NL,P} + (0.3P + 0.7) \cdot f_{NP,P}}{Y} \right) \right] \cdot \frac{1}{PR_P}$ where subscript T and P refer to tissue and plasma; fu is the fraction unbound drug in plasma and PR is albumin or lipoprotein concentration.

By substituting Eq. 19–22 into Eq. 18, predicted K_{pu} in each organ was obtained:

$$K_{pu} = \frac{C_T}{Cu_p} = \frac{X}{Y}\cdot f_{\mathrm{IW}} + f_{\mathrm{EW}} + \left[\frac{1}{f_u} - 1 - \left(\frac{P\cdot f_{\mathrm{NL},P} + (0.3P + 0.7)\cdot f_{\mathrm{NP},P}}{Y}\right)\right]\cdot\frac{PR_T}{PR_P} + \frac{P\cdot f_{\mathrm{NL}} + (0.3P + 0.7)\cdot f_{\mathrm{NP}}}{Y}. \quad (23)$$

Predicted tissue-to-plasma partition coefficient (K_{pu}) in each organ was calculated based on the Eq. 23 using tissue composition data from the literature (15,16).

Moreover, the octanol/water partition coefficient ($P_{o/w}$) was considered to use in non-adipose tissues but the vegetable oil/water partition coefficient ($P_{vo/w}$) was used for adipose tissue since vegetable oil represents natural lipid such as adipose tissue better than octanol (17). The linear relationship between experimental data of log $P_{vo/w}$ and log $P_{o/w}$ in organic chemicals including weak acids, bases, and neutral molecules was used to determine $P_{vo/w}$ based on $P_{o/w}$ as the following equation (18):

$$logP_{vo/w} = \left(1.115\cdot logP_{o/w}\right) - 1.35\,(n = 104, r = 0.99). \quad (24)$$

The clearance and distribution parameters were optimized according to a procedure from Peters (19) wherein the K_{pu} was scaled to get the best fit with the observed curve. A model optimization based on K_{pu} was conducted using the R-language based Advanced Modeling and Simulation Tool Kit (AMASTK, UI Copyright 2012). The optimization results showed an estimate of 4.52 for a scaling factor, which when incorporated into a PBPK model simulation demonstrated reasonable agreement between model-predicted curve and published pharmacokinetic profile (20) as shown in Fig. 3.

This PBPK disposition model was used for all reference and test emulsion product comparisons.

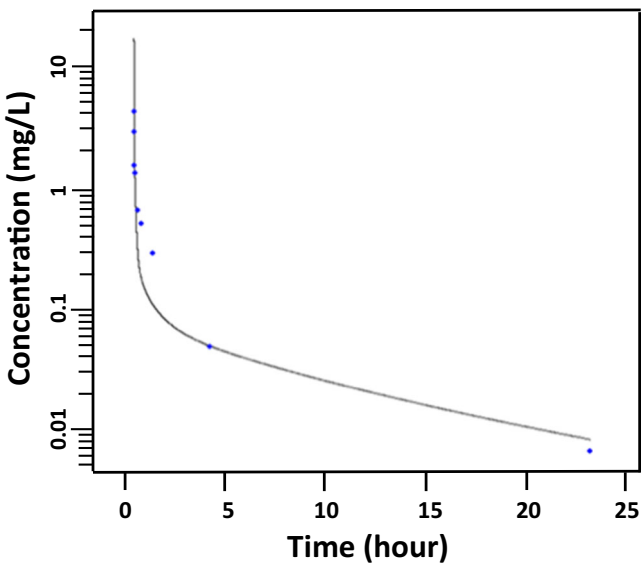

Fig. 3. Optimized PBPK model for propofol disposition using data from Doenicke *et al.* (20)

Methods for Comparator Computations

Three levels of comparisons were made for each pair of reference and test emulsion product (Fig. 1). PSD comparisons included overlap metrics (OVL and PROB) and median and span ratios. The simulated *in vitro* release profiles were compared using both similarity factor (f_2) and fractional release time ratios. Tradition bioavailability metrics (AUC, C_{max} and T_{max} ratios) were used to compare blood concentration-time profiles in accordance with US-FDA guidance (21) to assign BE or lack of BE.

PSD Overlap Comparators

Two metrics (OVL and PROB) were used to compare similarity of the PSD based on their extent of overlap.

OVL is a measure of a common area between two distributions. OVL is defined as (22).

$$\mathrm{OVL} = \int \min(f_1(x), f_2(x))dx \quad (25)$$

where $f_1(x)$ and $f_2(x)$ are probability (density) functions of reference and test drug products, respectively.

The value of OVL is bounded between 0 and 100% (0–1 in fractional terms). When there is no overlap between both distributions, the OVL value is 0% (or 0). In contrast, the OVL value will be 100% (or 1) when both distributions are identical as shown in Fig. 4.

PROB is a positional overlap metric that describes the probability that a particle randomly chosen from a test product distribution will be greater in size than a particle in the reference product distribution. It is computed using the following equation (23):

$$\mathrm{PROB} = \int (1 - F_1(x)) f_2(x)dx \quad (26)$$

where $F_1(x)$ is cumulative probability (density) function of test product distribution and $f_2(x)$ is probability (density) functions of reference product distribution, respectively.

As seen in Fig. 5, the value of PROB is also bounded in a range of 0–100% (0–1 in fractional terms). The PROB value is 0% (or 0) when the PSDs do not overlap and the test product distribution is completely to the left of the reference product PSD. The value of PROB will be 100% (or 1) if the PSDs do not overlap as well but the test product distribution is completely to the right of the reference product distribution. However, if both PSDs are identical, the PROB value will be 50% (or 0.5).

Median and Span Comparators

The median of PSD is a particle size at 50% of a cumulative size distribution. The median is also known as D_{50}. The ratio of the test to reference product median was used as a PSD metric.

The width of PSD is described by the span.

$$\mathrm{span} = \frac{D_{90} - D_{10}}{D_{50}} \quad (27)$$

where D_{90}, D_{10}, and D_{50} represent particle size at 90, 10, and 50% (median) in a cumulative size distribution, respectively. The ratio of the test to reference product span was used as a PSD metric.

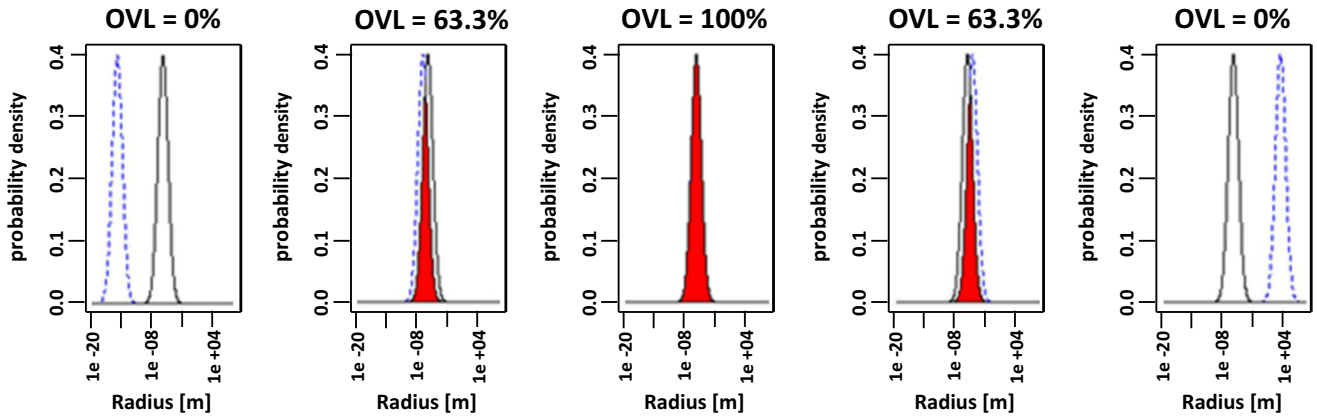

Fig. 4. Illustrations of OVL values as a function of the degree of overlap between two distributions

Release Rate Comparators

The f_2 metric (similarity factor) has been included in a number of FDA guidance documents (24–28). The f_2 metric was described by Moore and Flanner (29) and is a logarithmic transformation of the average sums of the squared vertical distances between the reference and test product mean values at selected time points as expressed in the following equation:

$$f_2 = 50 \cdot \log_{10}\left[1 + \frac{1}{n}\sum_{t=1}^{n}(R_t - T_t)^2\right]^{-0.5} \times 100 \tag{28}$$

where n is a number of sampling time point; R_t and T_t are the release values of reference and test drug products at the same time point. In this study, five time points were used at 10, 25, 50, 75, and 85% release of the reference drug product since the f_2 values are sensitive to the number of data points (30).

The value of f_2 can be in a range of 0–100. When both reference and test product mean profiles are identical, the f_2 is 100. If there is an average difference of 10% at all measured time points, the f_2 value will be 50. Therefore, FDA and Human Medicines Evaluation Unit of The European Agency for the Evaluation of Medicinal Products (EMEA) have suggested the criteria based on f_2 values that a similarity of two profiles will occur when the f_2 value is between 50 and 100 (31–33). Although the use of f_2 has been included in regulatory guidance, its utility has been questioned by pharmaceutical scientists and regulators (34,35).

Fractional time is the time required for a drug product to release a specific percent of drug and therefore represents a kinetic description of the release profile whereas the f_2 method collapses the time dependence by averaging a sum of differences over time. Fractional time comparisons have found limited use in regulatory guidance (*e.g.*, 85% of drug release in 30 min for BCS class I immediate release products (36)). In this work, five fractional times corresponding to drug releases of 10, 25, 50, 75, and 85% were estimated. They are denoted as t_{10}, t_{25}, t_{50}, t_{75}, and t_{85}, respectively. To compare fractional times between two drug products, fractional time ratios were calculated. These comparators provide an insight into kinetic differences of release mechanisms between reference and test drug products.

$$\text{Fractional time ratio} = \frac{t_{\text{test}}}{t_{\text{ref}}} \tag{29}$$

where $t_{\text{test/ref}}$ are fractional times of test and reference drug products at a certain percent release.

BE Comparators

According to regulatory guidance (37), an *in vivo* bioequivalence study is conducted in at least 12 healthy volunteers as a single-dose, crossover study. Pharmacokinetic parameters of both reference and test drug products, such as $AUC_{0\text{-}t}$, $AUC_{0\text{-}\infty}$, C_{max}, and T_{max}, are computed and used to construct 90% confidence intervals (CIs) of the ratios between reference and test product parameters. The CIs of

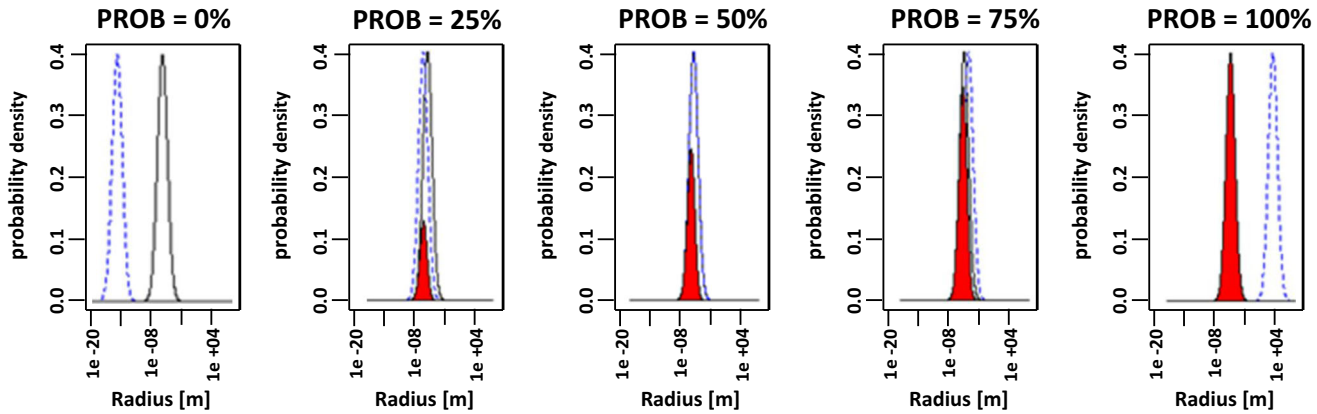

Fig. 5. Illustrations of PROB values as a function of the degree of overlap and position between two distributions

these ratios are then evaluated to determine whether they fall within a range of 0.80–1.25. If the intervals are within the limit, the test product is bioequivalent to the reference product. In this study, pharmacokinetic parameters from each product pair were compared as ratios between test and reference drug products to determine whether or not the product pair passed or failed the bioequivalence criteria of 0.80–1.25. The variability associated with clinical trial was not considered.

Monte Carlo Experiments

The utility of PSD and *in vitro* release comparator metrics for predicting bioequivalence was studied by generating 10,440 test/reference emulsion product pairs. Each pair was composed of an emulsion containing the same drug but with different PSD properties. These properties and the important subcutaneous-input parameters of the drug for each product pair were randomly selected as described below.

PSD Parameter Selection

The location, scale, and shape were selected to construct the reference and test product PSD. The location parameter (mean droplet size) for the reference product was either 10, 100, or 250 μm in radius thus covering a reasonable range of mean droplet sizes for subcutaneous administration. The location parameter for the test product was randomly selected within the range of 50 and 150% of the reference product location parameter. For scale parameters, reference and test values were each randomly selected from the range of 0.05 to 1. The shape parameters for both the reference and test values were also randomly selected from the range of − 3 to 3.

Release Rate Parameters

Three parameters govern drug release rates according to the Bikhazi/Higuchi model: particle size radii (r), diffusion coefficient (D), and partition coefficient (K). Particle size radii depend on PSDs which were selected as described above. The values of D and K were the same for both reference and test drug products since they are functions of the API. Distributions of typical D and K values were compiled from the literature (13) and used to estimate mean and variance values for normal distributions for typical D and log K values. These distributions were then randomly sampled to obtain values used to populate the release rate simulation for each pair of reference/test products (Fig. 6).

Subcutaneous-Input Parameters

To simulate pharmacokinetic responses for drug products with different PSDs and drug properties, the SQ input model was connected to a PBPK disposition model.

The subcutaneous permeability constant (k_{SQ}), and elimination fraction (EF) which regulate the transfer of drug from the subcutaneous to the venous blood compartment and first pass loss at the subcutaneous injection site were randomly selected using the following procedure.

The k_{SQ} parameter values were derived from the apparent permeability coefficient (P_{app}) based on Caco-2 studies for various drugs compiled from literature (38–54).

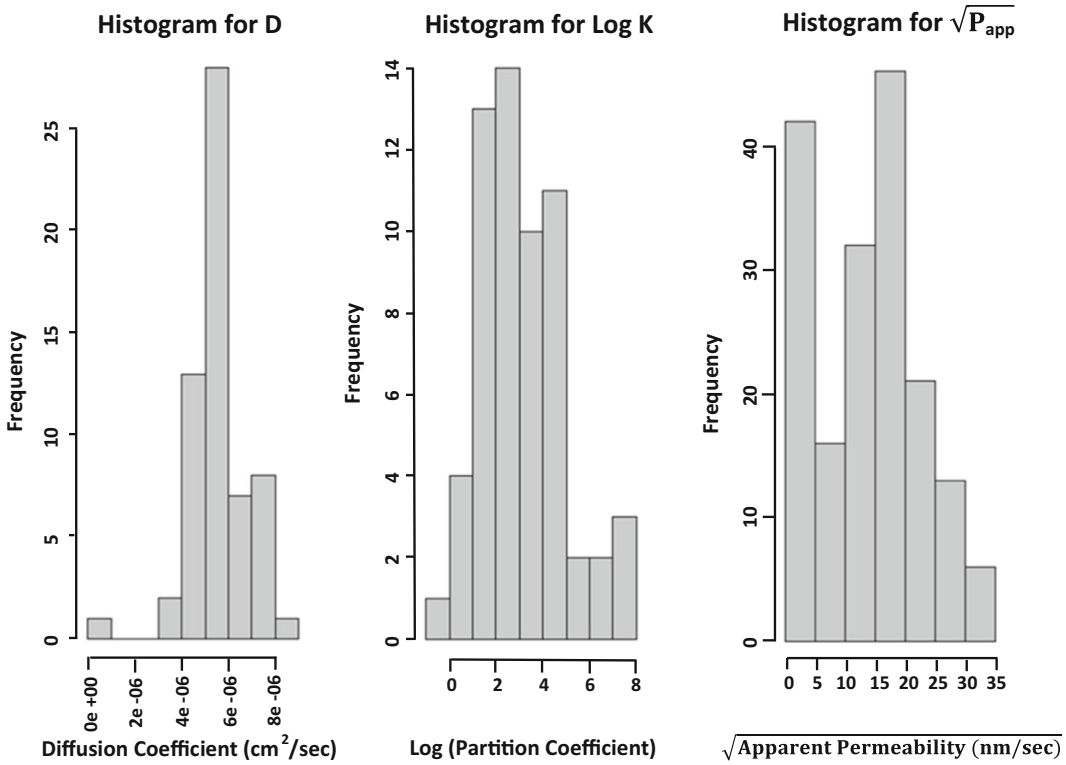

Fig. 6. Distributions of reported values for diffusion coefficients (D), partition coefficients (Log K) and apparent permeability coefficients ($P_{app}^{1/2}$) for drugs (13,38–54)

The distribution of these data ($P_{app}^{1/2}$) were normally distributed. Randomly selected $P_{app}^{1/2}$ was sampled from this normal distribution (Fig. 6). The selected P_{app} value was related to an effective permeability coefficient (P_{eff}) in accordance with the following equation (55):

$$\log P_{eff}(\mu m/\sec) = 0.4926 \cdot log P_{app}(nm/\sec) - 0.1454. \quad (30)$$

The estimated P_{eff} was divided by the thickness of subcutaneous layer (6 mm (56)) to obtain k_{SQ} value. The EF parameter was randomly selected for the range of 0.11 and 0.67 which corresponded to total bioavailability of 60–90%.

Methods for Correlating Product Comparators to Bioequivalence

Bioequivalence was determined by whether or not the ratio of test:reference product pharmacokinetic metric (AUC, C_{max}, and T_{max}) was within 0.8 to 1.25. If the ratio value was within that range then BE was assigned a value of 1 for "pass". Ratios outside the critical range were assigned a value of 0 for "fail". Logistic regression was utilized to correlate the numerical value of the PSD and release rate comparator to the probability for bioequivalence based on analysis of the 10,440 test/reference product pairs.

Logistic regression is a technique used when dependent variables are binary outcomes that may be related to a continuous independent variable. This analysis results in a probalistic estimate of the relationship between the dependent outcome and the regressor. In the current work, the probability of BE was estimated as a function of each PSD and release rate comparator value. Thus the probability of bioequivalence was described by estimating an intercept (β_0) and comparator coefficient (β) using the following model where x is the PSD or release comparator (57):

$$\text{Probability of bioequivalence} = \frac{1}{1 + e^{-(\beta_0 + \beta x)}}. \quad (31)$$

Some of the comparator values were transformed for the logistic regression analysis. PROB values were transformed into a unique value given by | PROB-0.5 | since PROB values

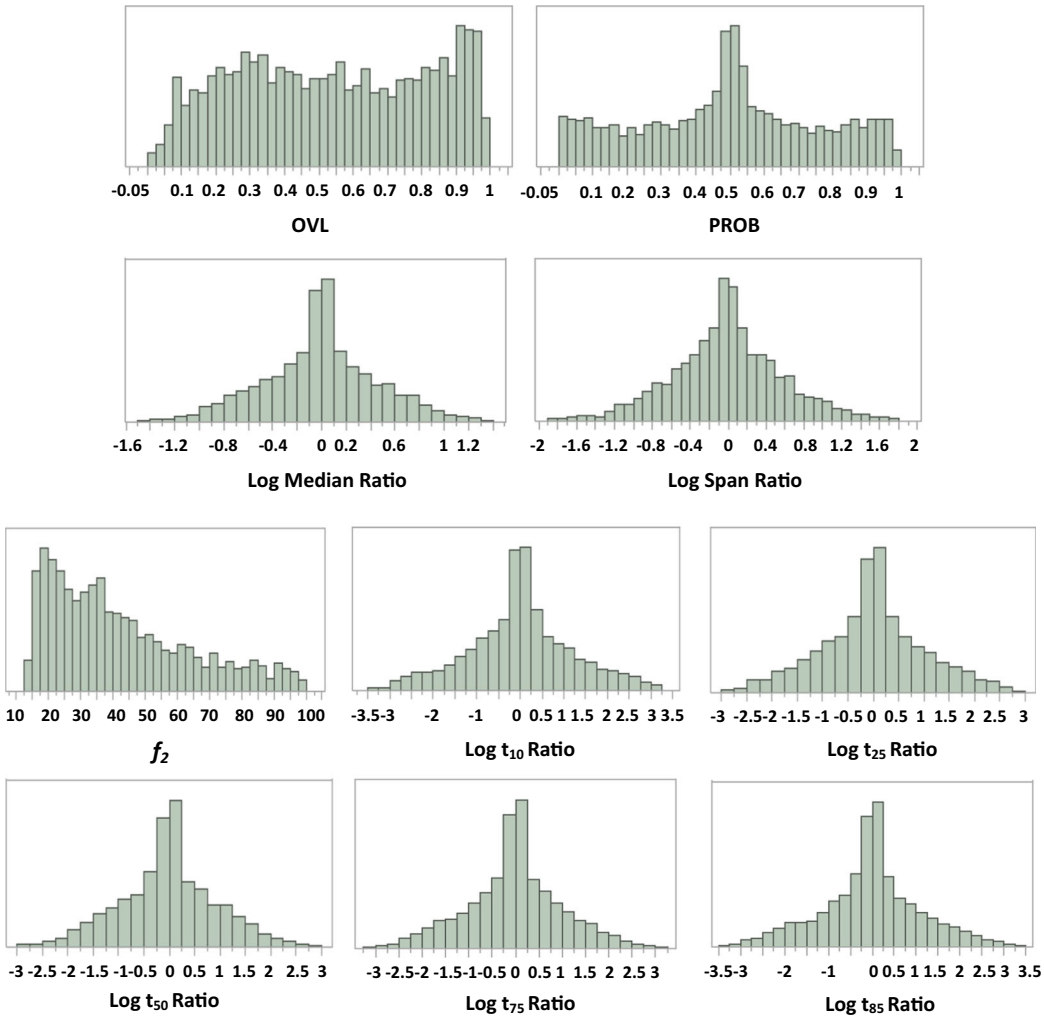

Fig. 7. Estimated values of PSD and release profile comparators from 10,440 simulated test/reference emulsion product pairs

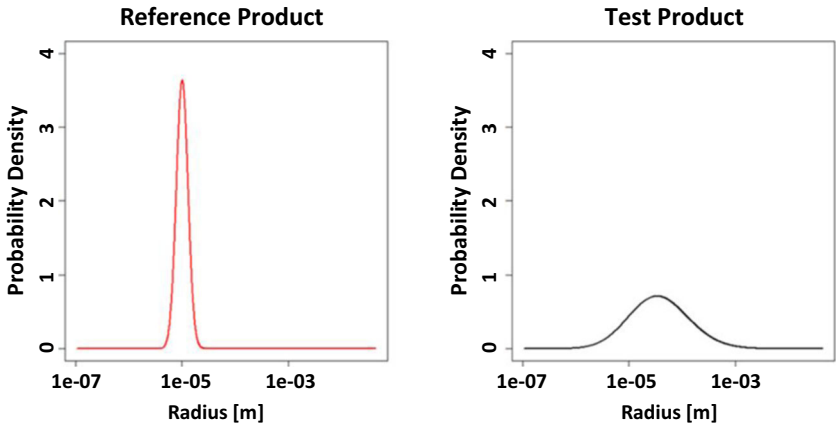

Fig. 8. Exemplary reference (left) and test (right) product PSD

describe both overlap and the position of overlap (*i.e.*, a location of test drug product is less or greater than reference drug product). For example, PROB values of 0.4 and 0.6 represent PSDs with the same amount of overlap but the median value of test drug product is less or greater than the reference drug product, respectively. The transformed values, | PROB-0.5 |, remove the positional aspect of the PROB statistic.

Similarly, the values of median, span, and five fractional time ratios were symmetrically distributed about the value of 0 (Fig. 7). To reflect the distance from the zero value, the absolute log comparator values were used.

JMP Pro 13.1 (SAS Institute Inc.) was used to estimate the intercept and comparator coefficient in the logistic regression model from each comparison metric with respect to each bioequivalence metric.

RESULTS

Example of a Test/Reference Pair Comparison

An example of the process used to create and evaluate reference and test product pair is described as follows:

Generating product pair: The values of D, K, P_{app} for reference drug product were 5.73×10^{-6} cm^2/s, 61,094, and 246.80 nm/s which were randomly selected from the distributions depicted in Fig. 6. The PSD parameters: location (ξ), scale (σ), and shape (α) for reference drug product were 10 μm, 0.11, and 0.09, respectively; the reference PSD is shown in Fig. 8 (left).

Creating test drug product: API properties of the test product were identical to reference drug product ($D = 5.73 \times 10^{-6}$ cm^2/s, $K = 61{,}094$, and $P_{app} = 246.80$ nm/s) but the PSD properties were randomly selected with different values of ξ, σ, and α at 14.99 μm, 0.69, and 1.04, respectively; the test PSD was shown in Fig. 8 (right).

Median and span values were measured from reference and test PSDs. After simulating release rate profiles of reference and test drug products using the modified Bikhazi/Higuchi model (Fig. 9), five fractional times were estimated (only the reference fractional time as displayed in Fig. 9). The blood concentration-time profiles of reference and test drug product were simulated using the subcutaneous-input PBPK model as illustrated in Fig. 10 and used to determine the AUC, C_{max}, and T_{max} values for each product.

Computing comparator values: The four PSD comparators were computed for the product pair: OVL, PROB, median ratio, and span ratio. Figure 11 shows PSD comparison of reference and test drug products based on OVL (left) and PROB (right). For the comparison of release rate profiles from reference and test drug products, f_2 and fractional time ratios were calculated. The calculation of f_2 is illustrated in Fig. 9. The five time points used in this calculation were selected from the reference product release profile at t_{10}, t_{25}, t_{50}, t_{75}, and t_{85}. Pharmacokinetic properties such as AUC, C_{max}, and T_{max} from test drug product were compared to reference drug product and categorized into two groups of "Pass" and "Fail" according to bioequivalence criteria of 0.80–1.25.

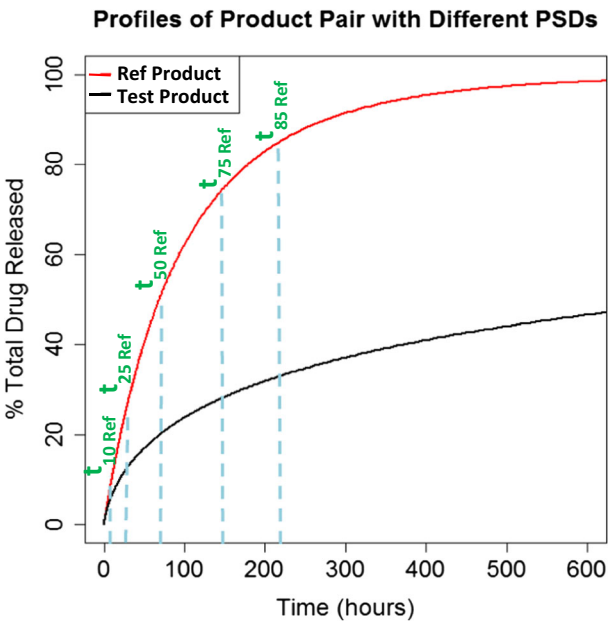

$$f_2 = 50 \times \log_{10}\left\{\left[1 + \tfrac{1}{5}((10-6.4)^2 + (25.1-12.2)^2 + (50-20)^2 + (75.2-28.5)^2 + (84.9-32.9)^2)\right]^{-0.5} \times 100\right\} = 23.08$$

Fig. 9. Simulated drug release profiles for exemplary test and reference emulsion products

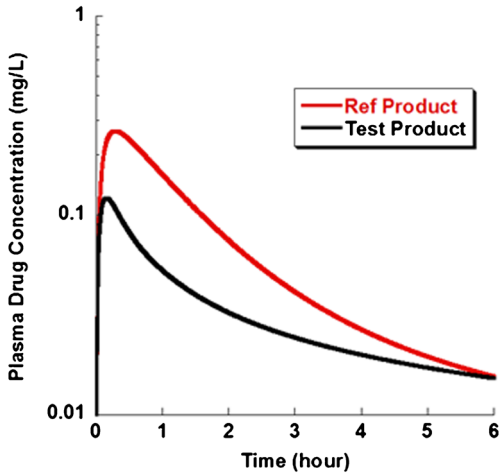

Fig. 10. Simulated blood concentration-time profiles for exemplary test and reference emulsion products

A summary table of the reference and test product values for this specific exemplary pair is shown in Table I. This entire process of creating a product pair and its performances, measuring and comparing the property values were repeatedly performed to construct the final data file for logistical regression.

Summary of Comparator Values

A total of 10,440 test/reference product pairs were evaluated using the procedure outlined in the preceding section. The distributions of PSD and release profile comparators resulting from the simulation of 10,440 test/reference emulsion product pairs are shown in Fig. 7.

Logistical Regression Results

The probability of BE was correlated to each PSD and release rate comparator values using logistical regression. The estimated parameters for the the regression model (Eq. 31) are shown in Table II for each PSD and release rate comparator. These values can be used to estimate the probability of BE at any given comparator value.

Exemplary logistic regression curves for OVL (PSD comparator) and f_2 (release profile comparator) with respect to AUC-based BE are presented in Fig. 12. In these logistic plots, each data point represents comparator value and categorized AUC bioequivalence from a product pair. On the right *y*-axis, a number of 1 or 0 indicates AUC bioequivalence "Pass" or "Fail". A tick mark on the axis also provides information about the total frequency of the "Pass/Fail" result for the entire data set of 10,440 test/reference product comparisons. As seen in the plots, the tick mark divided a length of the right *y*-axis into two sections: 78% for 1 and 22% for 0. This demonstrated that 78% of total product pairs passed AUC bioequivalence and 22% of total product pairs failed the AUC bioequivalence criterion.

The probability of AUC bioequivalence on the left *y*-axis is plotted as a function of comparator metric value on the *x*-axis. The table under each logistic plot is a test report showing whether or not the logistic regression model fits better than constant response probabilities which is similar to the analysis of variance for a continuous response model. However, a specific likelihood ratio chi-square test was used in the logistic analysis to evaluate how well the categorical model fits the data. The negative log-likelihood, sometimes called uncertainty in the sample, represents the negative sum of natural logs of the observed probabilities which is similar to sums of squares in continuous data. Reduced, full, and difference in model column indicate a model containing only an intercept, both intercept and comparator effect, and the difference of the negative log-likelihood from the reduced and full model, respectively. Twice the difference in the negative log-likelihood from fitting the model is a chi-square statistic which was used to investigate the hypothesis that a comparator has no effect on the AUC bioequivalence. Based on every table, PSD and release rate comparators have significant effects on AUC bioequivalence since the probability of getting a chi-square value greater than the one computed in ChiSquare column is less than 0.05 (shown in Prob>ChiSq column).

In Fig. 12 (top), the OVL metric showed a regression curve which increased as OVL values increased toward 1. This means product pairs had better chance to have a similar AUC if their OVL values were close to 1. In contrast, the regression curves of transformed PROB, median ratio, and span ratio demonstrated inverse relationships compared to OVL. These results indicated that the probability of AUC bioequivalence in product pairs was higher when their

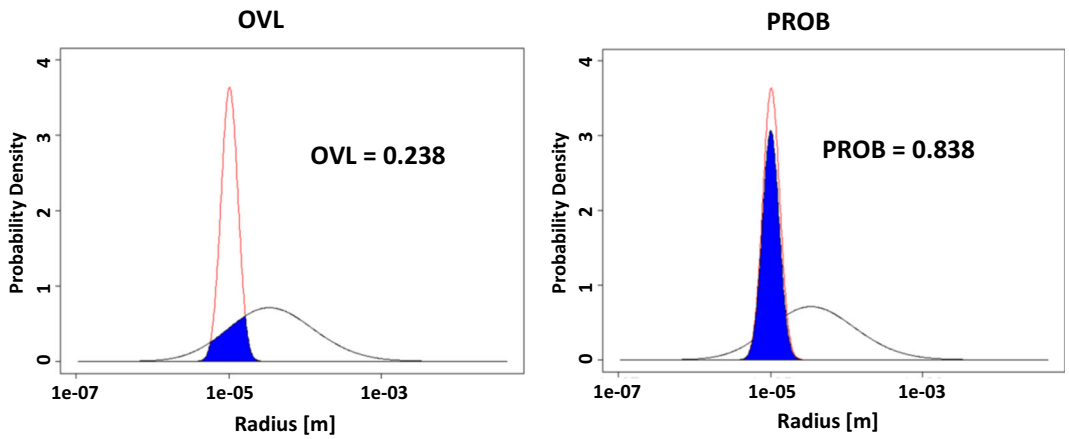

Fig. 11. PSD comparators (OVL and PROB) for exemplary emulsion products

Table I. Summary of Estimated Values and Comparator Values for Exemplary Test/Reference Product Pair

Metric	Reference product	Test product	Comparator values	Transformed value
OVL			0.24	0.24
PROB			0.84	0.84
Median	10	36	3.6	0.55
Span	0.66	5.4	8.1	0.91
f_2			23	23
t_{10} (h)	9.6	19	2.0	0.30
t_{25} (h)	27	111	4.1	0.62
t_{50} (h)	69	770	11	1.0
t_{75} (h)	150	5300	36	1.6
t_{85} (h)	220	15,000	71	1.8
AUC (mg/L*h)	0.88	0.70	0.80	Fail
C_{max} (mg/L)	0.26	0.12	0.46	Fail
T_{max} (h)	0.29	0.16	0.55	Fail

OVL, overlap coefficient; *PROB*, positional overlap metric; *AUC*, area under the concentration-time curve; C_{max}, maximum concentration; T_{max}, time of maximum concentration

transformed metric values tended toward 0. The difference in ascending and descending regression relationships is reflected in the sign of the comparator coefficient as shown in Table II.

Logistic regression curves of release profile comparator (f_2) were illustrated in Fig. 12 (bottom). The f_2 metric showed an ascending relationship with the probability of AUC bioequivalence similar to OVL metric.

DISCUSSION

Ability of Single Comparators (PSD and Release Profile) to Predict Bioequivalence

For each logistic regression analysis, two inverse predictions were performed to identify the critical values for each comparator with respect to each of the three bioequivalence metrics. The critical region was identified as the region of comparator values associated with a probability of bioequivalence equal or greater than a specific target value. Two target values of 0.85 and 0.9, corresponding to a probability of bioequivalence equal to 85 or 90%, were estimated.

Table III presents a critical value before and after transformation of each comparison metric when the probability of AUC bioequivalence was set at 0.85 and 0.9, respectively. Span ratio, t_{10} ratio, and t_{25} ratio could not predict AUC bioequivalence with the probability equal or greater than 0.85. In contrast, OVL, PROB, median ratio, f_2, t_{50} ratio, t_{75} ratio and t_{85} ratio could predict AUC bioequivalence prediction with the probability of at least 0.85. Values for OVL, f_2, t_{75} ratio, and t_{85} ratio which provided an AUC bioequivalence with the probability of equal or greater than 0.9 were also identified.

The critical regions for OVL, PROB, and median ratio using the 0.85 BE criterion were ≥ 0.72, 0.41–0.59, and 0.73–1.37, respectively. For release profile comparators, critical regions of f_2, t_{50} ratio, t_{75} ratio, and t_{85} ratio were ≥ 50.5, 0.56–1.80, 0.38–2.61, and 0.34–2.96, respectively. For AUC bioequivalence probability of 0.90, only four comparator metrics could be used to predict BE and

Table II. Estimated Logistic Regression Model Parameters for Each *In Vitro* Comparator with Respect to Each BE Metric

Comparator	AUC		C_{max}		T_{max}	
	Intercept (β_0)	Comp coeff. (β)	Intercept (β_0)	Comp coeff. (β)	Intercept (β_0)	Comp coeff. (β)
PSD comparison						
OVL	0.183	2.14	−2.25	3.40	−2.58	3.81
| PROB-0.5 |	2.04	−3.43	0.949	−6.74	0.747	−6.04
| Log median ratio |	2.00	−2.00	0.845	−4.08	0.646	−3.60
| Log span ratio |	1.73	−1.05	0.194	−1.34	0.222	−1.60
Release profile comparison						
f_2	−0.137	0.037	−2.90	0.061	−2.79	0.056
| Log t_{10} ratio |	1.50	−0.285	0.447	−1.00	0.681	−1.47
| Log t_{25} ratio |	1.66	−0.517	0.620	−1.42	0.720	−1.75
| Log t_{50} ratio |	1.97	−0.936	0.833	−1.97	0.659	−1.79
| Log t_{75} ratio |	2.20	−1.12	0.840	−1.90	0.469	−1.36
| Log t_{85} ratio |	2.22	−1.04	0.741	−1.58	0.362	−1.08

PSD, particle size distribution; *OVL*, overlap coefficient; *PROB*, positional overlap metric

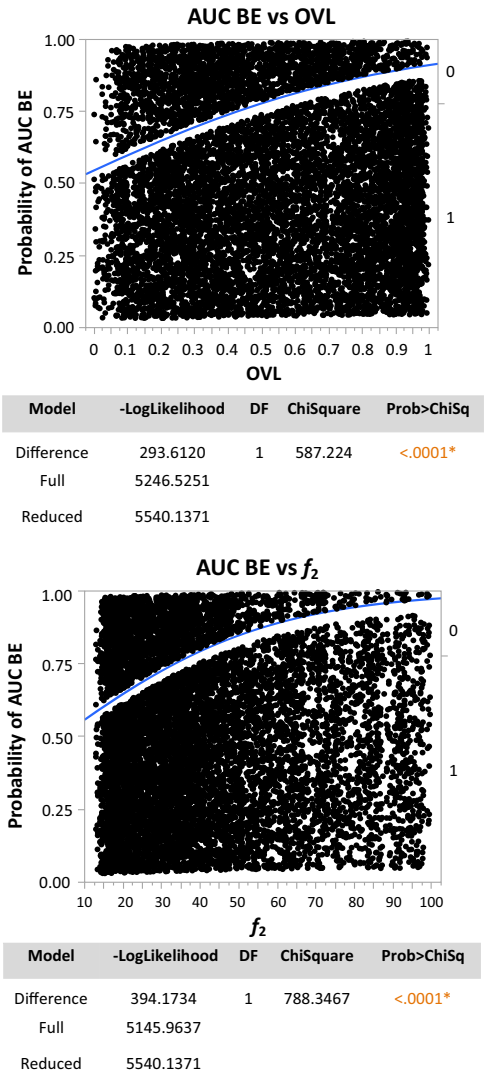

Fig. 12. Logistical regression model optimization for AUC-BE as functions of OVL and f_2 comparators using 10,440 test/reference emulsion product pairs

their critical regions were significantly narrower. For example, the critical regions of OVL, f_2, t_{75} ratio, and t_{85} ratio were ≥ 0.94, ≥ 63–100, 0.99–1.01, and 0.94–1.07, respectively.

The same process was also used to identify the critical region of each comparator metric with respect to C_{max} and T_{max} criteria. However, none of comparator metrics could predict bioequivalence based on C_{max} and T_{max} with the probability of equal or greater than 0.85, except f_2. For predicting C_{max} and T_{max} bioequivalence of at least 0.85, the critical regions of f_2 were ≥ 76.50 and ≥ 81, respectively. However, if the criterion was increased to at least 0.9, the critical regions of f_2 were changed to ≥ 84 and ≥ 89, respectively.

Ability of Comparators (PSD and Release Profile) Combinations to Predict Bioequivalence

The utility of using two comparators to predict BE was investigated since two comparators could be determined at different steps in drug product development process by measuring particle size distributions of the reference and test drug products and then by comparing release profiles of the product pairs.

To study the effect of combining metrics in predicting bioequivalence, the critical regions for PSD and release profile comparators were systematically combined and evaluated with respect to each of the three bioequivalence metrics. Then the probability of bioequivalence with the combinations of two comparator values within the critical ranges was determined. This analysis was performed by first sub-setting those product pairs which had PSD and release rate comparator values in the critical regions based on AUC bioequivalence. The resulting subset of product pairs was analyzed to determine the frequency of bioequivalence based on AUC, C_{max}, and T_{max} ratios.

OVL and PROB were chosen for PSD comparisons using their critical regions which predicted using AUC-BE probability ≥ 0.85. For release profile comparisons, f_2, t_{75} ratio, and t_{85} ratio were selected and their critical regions which predicted AUC bioequivalence with the probability

Table III. Critical Values of *In Vitro* Comparators with Respect to the Probability of AUC Bioequivalence at 0.85 and 0.90

Comparator	Critical value at 0.85		Critical value at 0.90	
	Transformed	Original	Transformed	Original
PSD comparison				
OVL	–	0.722	–	0.938
PROB	0.090	0.410, 0.590	–	–
Median ratio	0.137	0.729, 1.37	–	–
Span ratio	–	–	–	–
Release profile comparison				
f_2	–	50.5	–	63.0
t_{10} ratio	–	–	–	–
t_{25} ratio	–	–	–	–
t_{50} ratio	0.256	0.555, 1.80	–	–
t_{75} ratio	0.417	0.383, 2.61	0.0045	0.990, 1.01
t_{85} ratio	0.471	0.338, 2.96	0.0276	0.938, 1.07

PSD, particle size distribution; *OVL*, overlap coefficient; *PROB*, positional overlap metric

Table IV. Summary of the Probability of BE with Combinations of *In Vitro* Comparators Values in the Critical Range

Combined metric	No. of pairs	Probability of bioequivalence		
		AUC	C_{max}	T_{max}
OVL + f_2	2662	0.94	0.77	0.75
OVL + f_2*	1770	0.95	0.86	0.83
OVL + t_{75} ratio	2853	0.93	0.73	0.72
OVL + t_{85} ratio	2835	0.93	0.73	0.72
PROB + f_2	2754	0.93	0.78	0.73
PROB + f_2*	1851	0.95	0.86	0.82
PROB + t_{75} ratio	2856	0.93	0.76	0.70
PROB + t_{85} ratio	2661	0.93	0.77	0.72

OVL, overlap coefficient; *PROB*, positional overlap metric

of equal or greater than 0.85 were used in conjunction with critical regions from PSD comparison metrics. In addition, a critical region of f_2 which predicted AUC bioequivalence with the probability of equal or greater than 0.90 (f_2*) was also used along with critical regions from the PSD comparison metrics.

The results of this analysis are shown in Table IV. Of the original data pools containing 10,440 pairs, between 2600 and 2900 pairs had both a PSD and release profile comparator value in the critical 0.85 BE probability range. Within this subset, the probability of BE-based AUC, C_{max}, and T_{max} ratios was ≥ 0.93, ≥ 0.73, and ≥ 0.70, respectively. When f_2* was used in combination with OVL or PROB, 1800 product pairs were identified with the probability of BE based on AUC, C_{max}, and T_{max} ratios was 0.95, 0.86, and 0.82, respectively. Thus, the use of two product comparators appeared to offer greater utility in predicting bioequivalence then the use of single comparators.

CONCLUSION

The potential utility of using either or both PSD-based and release profile-based comparators for predicting bioequivalence may have role in generic product development. The process described herein of combining release rate, pharmacokinetic input, and disposition models to conduct Monte Carlo simulation experiments would appear to a reasonable first step. The application of these results presented herein is limited to emulsion formulations administered by subcutaneous route. Since the emulsion droplet PSDs were assumed to be constant after administration and release rates depended only on the initial droplet sizes, these assumptions are insufficient to describe drug behavior in other formulations such as suspensions wherein drug particle PSDs change over time as the particles erode during drug release. The complications involved with time-dependent PSD changes may be especially important for oral drug bioavailability wherein transit time, pH, transporter, and metabolic gradient in the GI tract are all relevant to drug absorption. In order to be considered reliable and more broadly applicable for other dosage forms and routes of administration, the models used for drug release, input, and disposition require considerable elaboration and refinement to incorporate the current understanding of bioavailability. Moreover, the influence of drug disposition kinetics on the results presented here requires additional consideration. Nonetheless, any attempt to leverage *in vitro* drug product testing *in lieu of* clinical trials with its inherent variability and the difficulty of conducting human studies is worth careful consideration and further study.

FUNDING INFORMATION

The authors gratefully acknowledge funding from the US-FDA and the National Institute of Pharmaceutical Technology and Education through contract #5U01FD004275-03; NIPTE-2013-002.

REFERENCES

1. Crowder TM, Hickey AJ, Louey MD, Orr NA. Guide to pharmaceutical particulate science. London: Interpharm/CRC; 2003.
2. U.S. National Archives and Records Administration. Title 21: Food and drugs. Chapter1-Food and Drug Administration. Code of Federal Regulations: part 320-bioavailability and bioequivalence requirements. 2017.
3. Food and Drug Administration. Draft guidance on cyclosporine: emulsion form/ophthalmic route. 2013.
4. Azzalini A, Capitanio A. The skew-normal and related families: Cambridge University Press; 2014. URL https://www.R-project.org/
5. Bikhazi AB, Higuchi WI. Interfacial barriers to the transport of sterols and other organic compounds at the aqueous polysorbate 80-hexadecane Interface. Biochim Biophys Acta Biomembr. 1971;233(3):676–87.
6. Sweeney R, Langenberg JP, Maxwell DM. A physiologically based pharmacokinetic (PB/PK) model for multiple exposure routes of soman in multiple species. Arch Toxicol. 2006;80(11):719–31.
7. Pamela N, Roy L, Celin D, Diana I, Emma P, Ian B, *et al*. Tolerability of Velcade (Bortezomib) subcutaneous administration using a maximum volume of 3 mL per injection site. J Oncol Pharm Pract. 2015;21(4):285–92.
8. Nguyen HQ, Stamatis SD, Kirsch E. A novel method for assessing drug degradation product safety using physiologically-based pharmacokinetic models and stochastic risk assessment. J Pharm Sci. 2015;104(9):3101–19.
9. Valentin J. Basic Anatomical and Physiological data for use in radiological protection: reference values. A report of age- and gender-related differences in the anatomical and physiological characteristics of reference individuals. ICRP Publication 89. Ann ICRP. 2002;32(3–4):5–265.
10. Drugs.com. Diprivan Information from Drugs.com. https://www.drugs.com/diprivan.html.
11. Gill KL, Houston JB, Galetin A. Characterization of in vitro Glucuronidation clearance of a range of drugs in human kidney microsomes: comparison with liver and intestinal glucuronidation and impact of albumin. Drug Metab Dispos. 2012;40(4):825–35.
12. Hospira. Propofol Injectable Emulsion. https://www.pattersonvet.com/msds/078889390.
13. Avdeef A, Nielsen PE, Tsinman O. PAMPA-a drug absorption in vitro model 11. Matching the in vivo unstirred water layer thickness by individual-well stirring in microtitre plates. Eur J Pharm Sci. 2004;22(5):365–74.
14. Gill KL, Gertz M, Houston JB, Galetin A. Application of a physiologically based pharmacokinetic model to assess propofol hepatic and renal glucuronidation in isolation: utility of in vitro and in vivo data. Drug Metab Dispos. 2013;41(4):744–53.
15. Rodgers T, Leahy D, Rowland M. Physiologically-based pharmacokinetic modeling 1: predicting the tissue distribution of moderate-to-strong bases. J Pharm Sci. 2005;94:1259–76.
16. Rodgers T, Rowland M. Physiologically-based pharmacokinetic modeling 2: predicting the tissue distribution of acids, very weak bases, neutrals and zwitterions. J Pharm Sci. 2006;95(6):1238–57.
17. Poulin P, Schoenlein K, Theil F-P. Prediction of adipose tissue:plasma partition coefficients for structurally unrelated drugs. J Pharm Sci. 2001;90(4):436–47.
18. Poulin P, Theil FP. Prediction of pharmacokinetics prior to in vivo studies. 1. Mechanism-based prediction of volume of distribution. J Pharm Sci. 2002;91(1):129–56.
19. Peters SA. Evaluation of a generic physiologically based pharmacokinetic model for lineshape analysis. Clin Pharmacokinet. 2008;47(4):261–75.
20. Doenicke AW, Roizen MF, Rau J, O'Connor M, Kugler J, Klotz U, *et al*. Pharmacokinetics and pharmacodynamics of propofol in a new solvent. Anesth Analg. 1997;85(6):1399–403.
21. Food and Drug Administration. Guidance for Industry: Bioequivalence Guidance. 2006.

22. Inman HF, Bradley EL. The overlapping coefficient as a measure of agreement between probability distributions and point estimation of the overlap of two normal densities. Commun Stat Theory Methods. 1989;18(10):3851–74.
23. Gastwirth JL. Statistical measures of earnings differentials. Am Stat. 1975;29(1):32–5.
24. Food and Drug Administration. Guidance for Industry: Bioavailability and Bioequivalence Studies for Orally Administered Drug Products-General Considerations. 2003.
25. Food and Drug Administration. Guidance for Industry: immediate-release solid oral dosage forms: scale-up and post-approval changes: chemistry, manufacturing and controls, in vitro dissolution testing, and in vivo bioequivalence documentation. 1995.
26. Food and Drug Administration. Guidance for industry: Dissolution testing of immediate release solid oral dosage forms. 1997.
27. Food and Drug Administration. Guidance for Industry: SUPAC-MR: modified release solid oral dosage forms. Scale-up and post-approval changes: chemistry, manufacturing, and controls; in vitro dissolution testings and in vivo bioequivalence documentation. 1997.
28. Food and Drug Administration. Guidance for Industry: Extended release oral dosage forms: development, evaluation, and application of in vitro/in vivo correlations. 1997.
29. Moore JW, Flanner HH. Mathematical comparison of dissolution profiles. Pharm Technol. 1996:64–74.
30. O'Hara T, Dunne A, Butler J, Devane J. A review of methods used to compare dissolution profile data. Pharmaceutical Science & Technology Today. 1998;1(5):214–23.
31. Duan J, Riviere K, Marroum P. In vivo bioequivalence and in vitro similarity factor (f2) for dissolution profile comparisons of extended release formulations: how and when do they match? Pharm Res. 2011;28(5):1144–56.
32. Xie F, Ji S, Cheng Z. In vitro dissolution similarity factor (f2) and in vivo bioequivalence criteria, how and when do they match? Using a BCS class II drug as a simulation example. Eur J Pharm Sci. 2015;66(0):163–72.
33. Costa P, Sousa Lobo JM. Modeling and comparison of dissolution profiles. Eur J Pharm Sci. 2001;13(2):123–33.
34. Shah VP, Tsong Y, Sathe P, Liu JP. In vitro dissolution profile comparison-statistics and analysis of the similarity factor, f2. Pharm Res. 1998;15(6):889–96.
35. LeBlond D, Altan S, Novick S, Peterson J, Shen Y, Yang H. In vitro dissolution curve comparisons: a critique of current practice. Dissolution Technologies. 2016;23:14–23.
36. Food and Drug Administration. Guidance for Industry: dissolution testing and specification criteria for immediate-release solid oral dosage forms containing biopharmaceutics classification system class 1 and 3 drugs. 2015.
37. Food and Drug Administration. Guidance for industry: statistical approaches to establishing bioequivalence. 2001.
38. Artursson P. Epithelial transport of drugs in cell culture. I: a model for studying the passive diffusion of drugs over intestinal absorbtive (Caco-2) cells. J Pharm Sci. 1990;79(6):476–82.
39. Artursson P, Karlsson J. Correlation between oral drug absorption in humans and apparent drug permeability coefficients in human intestinal epithelial (Caco-2) cells. Biochem Biophys Res Commun. 1991;175(3):880–5.
40. Haeberlin B, Rubas W, Nolen IIIHW, Friend DR. In vitro evaluation of dexamethasone-β-D-glucuronide for colon-specific drug delivery. Pharm Res. 1993;10(11):1553–62.
41. Rubas W, Jezyk N, Grass GM. Comparison of the permeability characteristics of a human colonic epithelial (Caco-2) cell line to colon of rabbit, monkey, and dog intestine and human drug absorption. Pharm Res. 1993;10(1):113–8.
42. Hovgaard L, Brøndsted H, Buur A, Bundgaard H. Drug delivery studies in Caco-2 monolayers. Synthesis, hydrolysis, and transport of O-cyclopropane carboxylic acid ester prodrugs of various β-blocking agents. Pharm Res. 1995;12(3):387–92.
43. Augustijns P, D'Hulst A, Van Daele J, Kinget R. Transport of artemisinin and sodium artesunate in Caco-2 intestinal epithelial cells. J Pharm Sci. 1996;85(6):577–9.
44. Collett A, Sims E, Walker D, He Y-L, Ayrton J, Rowland M, *et al.* Comparison of HT29-18-C1 and Caco-2 cell lines as models for studying intestinal paracellular drug absorption. Pharm Res. 1996;13(2):216–21.
45. Yee S. In vitro permeability across Caco-2 cells (colonic) can predict in vivo (small intestinal) absorption in man-fact or myth. Pharm Res. 1997;14(6):763–6.
46. Yazdanian M, Glynn SL, Wright JL, Hawi A. Correlating partitioning and Caco-2 cell permeability of structurally diverse small molecular weight compounds. Pharm Res. 1998;15(9):1490–4.
47. Zhu C, Jiang L, Chen T-M, Hwang K-K. A comparative study of artificial membrane permeability assay for high throughput profiling of drug absorption potential. Eur J Med Chem. 2002;37(5):399–407.
48. Saha P, Kou JH. Effect of bovine serum albumin on drug permeability estimation across Caco-2 monolayers. Eur J Pharm Biopharm. 2002;54(3):319–24.
49. Camenisch G, Alsenz J, van de Waterbeemd H, Folkers G. Estimation of permeability by passive diffusion through Caco-2 cell monolayers using the drugs' lipophilicity and molecular weight. Eur J Pharm Sci. 1998;6(4):313–9.
50. Takano R, Sugano K, Higashida A, Hayashi Y, Machida M, Aso Y, *et al.* Oral absorption of poorly water-soluble drugs: computer simulation of fraction absorbed in humans from a miniscale dissolution test. Pharm Res. 2006;23(6):1144–56.
51. Yang Y, Faustino PJ, Volpe DA, Ellison CD, Lyon RC, Yu LX. Biopharmaceutics classification of selected β-blockers: solubility and permeability class membership. Mol Pharm. 2007;4(4):608–14.
52. Sjögren E, Westergren J, Grant I, Hanisch G, Lindfors L, Lennernäs H, *et al.* In silico predictions of gastrointestinal drug absorption in pharmaceutical product development: application of the mechanistic absorption model GI-Sim. Eur J Pharm Sci. 2013;49(4):679–98.
53. Schipper NGM, Osterberg T, Wrange U, Westberg C, Sokolowski A, Rai R, *et al.* In vitro intestinal permeability of factor Xa inhibitors: influence of chemical structure on passive transport and susceptibility to efflux. Pharm Res. 2001;18(12):1735–41.
54. National Center for Biotechnology Information. PubChem compound database. Available from: https://pubchem.ncbi.nlm.nih.gov/.
55. Gertz M, Harrison A, Houston JB, Galetin A. Prediction of human intestinal first-pass metabolism of 25 CYP3A substrates from in vitro clearance and permeability data. Drug Metab Dispos. 2010;38(7):1147–58.
56. Schmitt JM, Zhou GX, Walker EC. Multilayer model of photon diffusion in skin. J Opt Soc Am A. 1990;7(11):2141–53.
57. Shalizi CR. Logistic Regression. In: Advanced data analysis from an elementary point of view. Carnegie Mellon University; 2017. p. 251–280.